VIP *Very Important Paper*

Sequence-Selective Covalent CaaX-Box Receptors Prevent Farnesylation of Oncogenic Ras Proteins and Impact MAPK/PI3 K Signaling

Matthias Franz,[a] Britta Mörchen,[b] Carsten Degenhart,[c] Daniel Gülden,[a] Oleksandr Shkura,[d] Dirk Wolters,[d] Uwe Koch,[c] Bert Klebl,[c] Raphael Stoll,[d] Iris Helfrich,[b] and Jürgen Scherkenbeck*[a]

Oncogenic Ras proteins are implicated in the most common life-threatening cancers. Despite intense research over the past two decades, the progress towards small-molecule inhibitors has been limited. One reason for this failure is that Ras proteins interact with their effectors only via protein-protein interactions, which are notoriously difficult to address with small organic molecules. Herein we describe an alternative strategy, which prevents farnesylation and subsequent membrane insertion, a prerequisite for the activation of Ras proteins. Our approach is based on sequence-selective supramolecular receptors which bind to the C-terminal farnesyl transferase recognition unit of Ras and Rheb proteins and covalently modify the essential cysteine in the so-called CaaX-box.

Introduction

Ras-GTPases belong to the GTP-binding proteins that are involved in numerous cellular processes such as cell growth, cell regulation, and signal transduction. Mutations of the Ras isoforms K-Ras, H-Ras and N-Ras play a decisive role in lung, colorectal, and pancreatic cancer, the most common and life-threatening cancers overall. Hyperactive K-Ras is implicated in at least 80% of pancreas and around 50% of colorectal carcinoma.[1–4] Rheb (Ras homologue enriched in brain) belongs to a unique family within the Ras superfamily. Hyperactivation of Rheb causes the formation of benign hamartomatous tumors (tuberous sclerosis) in the brain, kidneys, lung or eyes.[5,6] In addition, Rheb is involved in the development of aggressive and drug-resistant lymphomas.[7] Though, Ras proteins are in principle "gold-targets" for the development of novel anti-cancer drugs medicinal chemists have tried unsuccessfully for decades to find an effective inhibitor.[8–10] A major cause for the failure of those direct targeting approaches is, that Ras proteins interact with their effectors via large surface interactions, which are difficult to block with small-molecule inhibitors. Only in the very recent past some promising lead-structures interfering with the Ras effector binding-sites, have been published.[11–16]

Ras proteins consist of two domains, the highly conserved G-domain, which has been the target of almost all direct Ras inhibitor strategies and a hypervariable C-terminal domain consisting of residues 165–188/189 (Figure 1). This short, highly unstructured H-domain significantly diverges in sequence among Ras proteins and contains a C-terminal signal sequence, the so-called CaaX-box ("C" represents Cys, "a" an aliphatic amino acid, and "X" Ser or Met), which is subject to posttranslational farnesylation. The prenylation of the CaaX-box cysteine is a prerequisite for correct membrane localization and full functionality of Ras proteins. Additional cysteine residues in the H-domain of N-Ras and K-Ras4A are single or in the case of H-Ras double palmitoylated.[1,17–19] Only K-Ras4B uses a polybasic hexalysine (Lys 175–180) sequence for membrane association in

[a] M. Franz, D. Gülden, Prof. Dr. J. Scherkenbeck
Faculty of Mathematics and Natural Sciences
University of Wuppertal
42119 Wuppertal (Germany)
E-mail: scherkenbeck@uni-wuppertal.de
[b] B. Mörchen, Dr. I. Helfrich
Vascular Oncology & Metastasis
University Hospital Essen
45147 Essen (Germany)
[c] C. Degenhart, Dr. U. Koch, Dr. B. Klebl
Lead Discovery Center GmbH
44227 Dortmund (Germany)
[d] O. Shkura, Dr. D. Wolters, Prof. Dr. R. Stoll
Faculty of Chemistry and Biochemistry
Ruhr-University Bochum
44780 Bochum (Germany)

Supporting information for this article is available on the WWW under https://doi.org/10.1002/cmdc.202100167

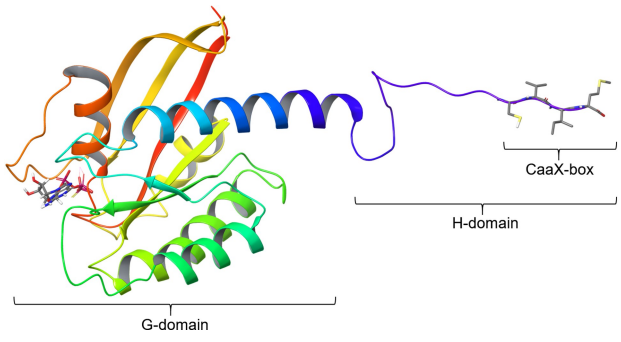

Figure 1. Structure of K-Ras4B(GTP).

addition to the farnesylated CaaX-box. Albeit, all post-translational Ras-processing enzymes have been investigated, FTase turned out to be the most promising drug target.[20] FTase inhibitors (FTIs), such as Tipifarnib, Lonafarnib and some others entered clinical development.[21] However, the relevant CaaX-box cysteine can be alternatively prenylated by geranylgeranyltransferase. This limits the medical benefit of FTIs considerably.

A largely neglected strategy to interfere with the Ras-prenylation process comprises the sequence-selective molecular recognition of the CaaX-box of a Ras protein by a synthetic small receptor molecule and subsequent formation of a supramolecular complex that prevents farnesyl transferase from recognizing the CaaX-box and transferring the prenyl group onto the Cys residue. This molecular receptor strategy has at least in principle several advantages over conventional FTIs. First, toxic side-effects caused by unspecific blocking of different FTases are avoided. Second, farnesylation cannot be bypassed by palmitoylation or other prenylation processes, a major problem with FTIs, since the critical cysteine in the CaaX-box is masked and not accessible for any kind of modification. Depending on the length of those molecular receptors additional cysteines in the C-terminal region of H-Ras, K-Ras4A or N-Ras can be blocked. Third, it should be possible to find Ras-subtype specific receptors, since the CaaX-boxes of H-Ras, N-Ras and K-Ras differ significantly in their sequences. The proof of principle of this concept was demonstrated by Nestler et al., who identified a molecular forceps (**1**) from a huge combinatorial library of more than 150,000 compounds, which selectively prevented the farnesylation of H-Ras *in vitro* (Figure 2) by forming a supramolecular complex with the respective CaaX-box.[22] It was clearly shown that this effect was not due to inhibition of FTase by the molecular receptor. However, to get a 75% reduction of farnesylation, receptor concentrations of more than 250 μM ($IC_{50} > 100$ μM) were required, probably because the receptor lacks a strong carboxylate binding group. Nevertheless, the molecular receptor concept appears superior to conventional FTIs due to its potential for higher selectivity and prevention of alternative prenylation processes.

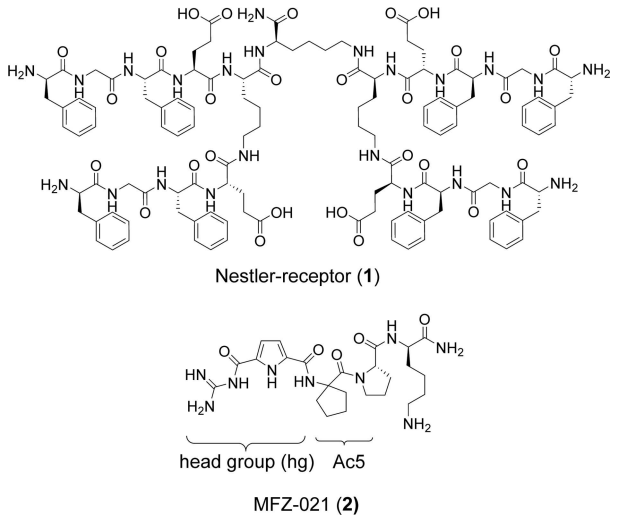

Figure 2. Structures of Nestler-receptor (**1**) and molecular forceps MFZ-021 (**2**).

The major driving force for molecular recognition of the CaaX-sequence is the formation of a salt-bridge between the C-terminal carboxylate and the protonated basic head-group of the receptor molecule. Several carboxylate recognizing motifs have been published in the past, one of the most efficient of which is a guanidiniopyrrole scaffold, developed by Schmuck.[23–25] In a foregoing work we described receptor molecules from a 8,000 member library based on the Schmuck head-group (Figure 2) which were significantly less complex in structure and showed improved CaaX-box binding compared to the Nestler receptor (Table 1).[26] K_a values of 30,000 M^{-1} and 19,800 M^{-1} were determined by NMR titration in an aqueous DMSO-water (6:4) solution for the Rheb CaaX-box peptides MFZ-021 (**2**) and MFZ-022 (**3**).[27] The CaaX-box of K-Ras4B represents a particular challenge for molecular recognition, since it consists exclusively of nonpolar residues. Not unexpected, a K_a value of only 4,100 M^{-1} was found for the best receptor MFZ-023 (**5**, Table 1).

In this paper we show that a sequence-selective covalent modification of the CaaX-box cysteine results in a considerably improved suppression of farnesylation and subsequently in modified MAPK/PI3K signaling in colon cancer $KRAS_{G13D}$ HCT116 as well as non-small cell lung cancer (NSCLC) $KRAS_{G12C}$ NCI-H358 cell lines.

Results and Discussion

Structure and activity of molecular receptors

The natural H-Ras CaaX-box substrate GCVLS binds to rat FTase with K_D values of 4 μM and 0.058 μM, depending on the absence or presence of farnesylpyrophosphate. A K_D value of 0.5 μM was measured for the H-Ras protein.[28] Not completely unexpected, the unmodified CaaX-Box receptors MFZ-021-023 (**2**–**5**) as well as the Nestler receptor **1**, used as benchmark, did not reduce CaaX-box farnesylation in the relevant range up to $IC_{50} \leq 30$ μM. The affinity of the unmodified molecular forceps is simply too low for a tight association with the CaaX-box in an

Table 1. NMR-determined K_a values of Rheb, H-Ras, and K-Ras4B receptors.

Receptor	K_a [M^{-1}][a]	K_a [M^{-1}][b]	K_a [M^{-1}][c]
Rheb CaaX-box:			
H_2NCO–D-Lys-L-Pro-AC5 C-hg (MFZ-021, **2**)	$\geq 10^5$	30,000	$> 5 \times 10^7$
H_2NCO–D-Lys-L-Pro-L-Lys-hg (MFZ-022, **3**)	$\geq 10^5$	19,800	3.0×10^5
H-Ras CaaX-box:			
H_2NCO–D-Leu-L-Ser-L-Ser-hg (PMD-139, **4**)	$\geq 10^5$	1,150	n.d.
K-Ras CaaX-box:			
H_2NCO–D-Lys-GABA–L-Lys-hg (MFZ-023, **5**)	$\geq 10^5$	4,100	n.d.

[a] K_a values for NMR titrations in [D_6]DMSO. [b] NMR titrations in [D_6]DMSO-H_2O 6:4. [c] UV titrations in DMSO. AC5 C: 1-Aminocyclopentanecarboxylic acid. hg: guanidiniopyrrole head group.

aqueous environment (Table 1). As the consequence, FTase, which binds with nanomolar K_D values to the CaaX-box recognition sequence, displaces the synthetic receptors, unless added in inacceptable high concentrations.

Therefore, derivatives of our receptors carrying covalent modifying groups were prepared by solid-phase synthesis and tested for their inhibition of farnesylation. Although fraught with concerns about toxicity, covalent drugs may provide significant advantages for patients such as higher potency and prolongation of therapeutic response.[29–33] While covalent modifying reagents have been developed for most amino acids with a functional group in the side-chain, the preferred target still is cysteine due to the specific properties of the sulfur atom, such as high nucleophilicity and a favourable pK_a which is fine-tuned by the protein-environment.[34,35] In our work, we used reversibly covalent modifying acrylamide, maleimide and thiol residues. The strong Michael acceptor maleimide has been shown to be highly specific for thiols between pH 6.5–7.5. The ε-amino group in Lys, for instance, reacts slower by a factor of 1000.

Remarkably, the L-Lys(Acr) modified receptors were inactive in the measured concentration range, regardless of whether the acryloyl residue was attached to the Lys of the original receptor (Table 2, Series 1,) or an additional Lys(Acr) was coupled to the unmodified receptor (Table 2, Series 2). Much more encouraging results were obtained with the maleimides which are known for their higher Michael-acceptor reactivity (Table 2, series 3). Excellent IC_{50} values in the range of 4.5–8.2 μM were found for K-Ras4B and on a comparable level (3.6–16.3 μM) also for Rheb while the inhibition of H-Ras was significantly weaker. The unmodified Rheb receptors MFZ-021 (**2**) and MFZ-022 (**3**) already showed the highest K_a values in NMR titration experiments (Table 1). Not unexpected, this motif extended by a Lys (Gly-Mi) residue afforded the best covalent Rheb farnesylation inhibitors MFZ-063 (**13**) and MFZ-065 (**15**). Disappointingly, these two molecular receptors turned out to be unselective for K-Ras4B and Rheb. Instead, MFZ-062 (**12**) and MFZ-066 (**16**) showed interesting selectivities by a factor of around two in favor of the K-Ras4B CaaX-box. Remarkably, the stereochemistry of the Lys(Gly-Mi) residue (series 3) contributes significantly to the overall activities but also to the observed selectivities of our molecular pincers. For instance, the (*D*)-enantiomer of Lys(Gly-Mi) provides stronger Rheb inhibitors, while the (*L*)-enantiomer results in higher selectivity for K-Ras4B. In contrast to the maleimides, the Cys containing receptors (Table 2, series 4 and 5) bind more selectively to the Caax-box of H-Ras. The best IC_{50} of 8.6 μM against H-Ras and a selectivity by a factor of 2–3 was found for compound MFZ-148 (**27**).

MFZ-105 (**7**) as all other acrylamides, which were already found inactive in the FTase assay, also do not react with either of the 11mer C-terminal cysteines of K-Ras4B, H-Ras, and Rheb at a concentration of 100 μM in PBS buffer at pH 7.4 (Figure 3). Even after 24 h, no Michael addition products were detected for all three CaaX-boxes. Instead, oxidative homo-dimerization products were formed. In contrast, thiol MFZ-115 (**23**) a representative of the Cys modified receptors, shows a slow but distinct formation of the heterodisulfides formed by the receptor thiol and the CaaX-box Cys (Figure 3). The C-terminal 11mer H-Ras peptide contains three Cys residues, in positions 4 (CaaX-box), 6, and 9 (counted from the C-terminus). It is all the

Table 2. FTase inhibition (IC_{50}, μM) of molecular CaaX-box receptors.

Receptor	K-Ras4B	H-Ras	Rheb
Series 1			
H_2NCO–D-Lys(Acr)-L-Pro-L-Lys-hg (MFZ-102, **6**)	>30	>30	>30
H_2NCO–D-Lys(Acr)-GABA–L-Lys-hg (MFZ-105, **7**)	>30	n.d.[a]	n.d.[a]
Series 2			
H_2NCO–L-Lys(Acr)-D-Lys-L-Pro-AC5 C-hg (MFZ-039, **8**)	>30	>30	>30
H_2NCO–D-Lys(Acr)-D-Lys-L-Pro-AC5 C-hg (MFZ-040, **9**)	>30	>30	>30
H_2NCO–L-Lys(Acr)-D-Lys-L-Pro-L-Lys-hg (MFZ-041, **10**)	>30	>30	25.3
H_2NCO–D-Lys(Acr)-D-Lys-L-Pro-L-Lys-hg (MFZ-042, **11**)	>30	>30	28.2
Series 3			
H_2NCO–L-Lys(Gly-Mi)-D-Lys-L-Pro-AC5 C-hg (MFZ-062, **12**)	4.7	14.5	9.0
H_2NCO–D-Lys(Gly-Mi)-D-Lys-L-Pro-AC5 C-hg (MFZ-063, **13**)	5.8	17.7	4.0
H_2NCO–L-Lys(Gly-Mi)-D-Lys-L-Pro-L-Lys-hg (MFZ-064, **14**)	8.2	22.4	16.3
H_2NCO–D-Lys(Gly-Mi)-D-Lys-L-Pro-L-Lys-hg (MFZ-065, **15**)	4.5	14.8	3.6
H_2NCO–L-Lys(Gly-Mi)-D-Lys-GABA–L-Lys-hg (MFZ-066, **16**)	5.0	16.3	11.7
H_2NCO–D-Lys(Gly-Mi)-D-Lys-GABA–L-Lys-hg (MFZ-067, **17**)	5.8	18.6	10.3
Series 4			
H_2NCO–D-Cys-L-Pro-AC5 C-hg (MFZ-110, **18**)	>30	25.3	>30
H_2NCO–D-Cys -L-Pro-L–Lys-hg (MFZ-111, **19**)	>30	13.3	>30
H_2NCO–D-Cys-GABA–L-Lys-hg (MFZ-112, **20**)	>30	14.7	>30
Series 5			
H_2NCO–L-Cys-D-Lys-L-Pro-AC5 C-hg (MFZ-113, **21**)	>30	22.0	>30
H_2NCO–D-Cys-D-Lys-L-Pro-AC5 C-hg (MFZ-114, **22**)	>30	13.0	24.8
H_2NCO–L-Cys-D-Lys-L-Pro-L–Lys-hg (MFZ-115, **23**)	>30	18.2	>30
H_2NCO–D-Cys-D-Lys-L-Pro-L–Lys-hg (MFZ-116, **24**)	>30	15.7	>30
H_2NCO–L-Cys-D-Lys-GABA–L-Lys-hg (MFZ-117, **25**)	26.3	15.5	25.0
H_2NCO–D-Cys-D-Lys-GABA–L-Lys-hg (MFZ-118, **26**)	>30	n.d.	>30
H_2NCO–L-Cys-D-Lys-L-Pro(4-F)-L–Lys-hg (MFZ-148, **27**)	17.2	8.6	25.2

[a] Not determined; poor curve fit. Acr: acrylamide. Mi: maleimide.

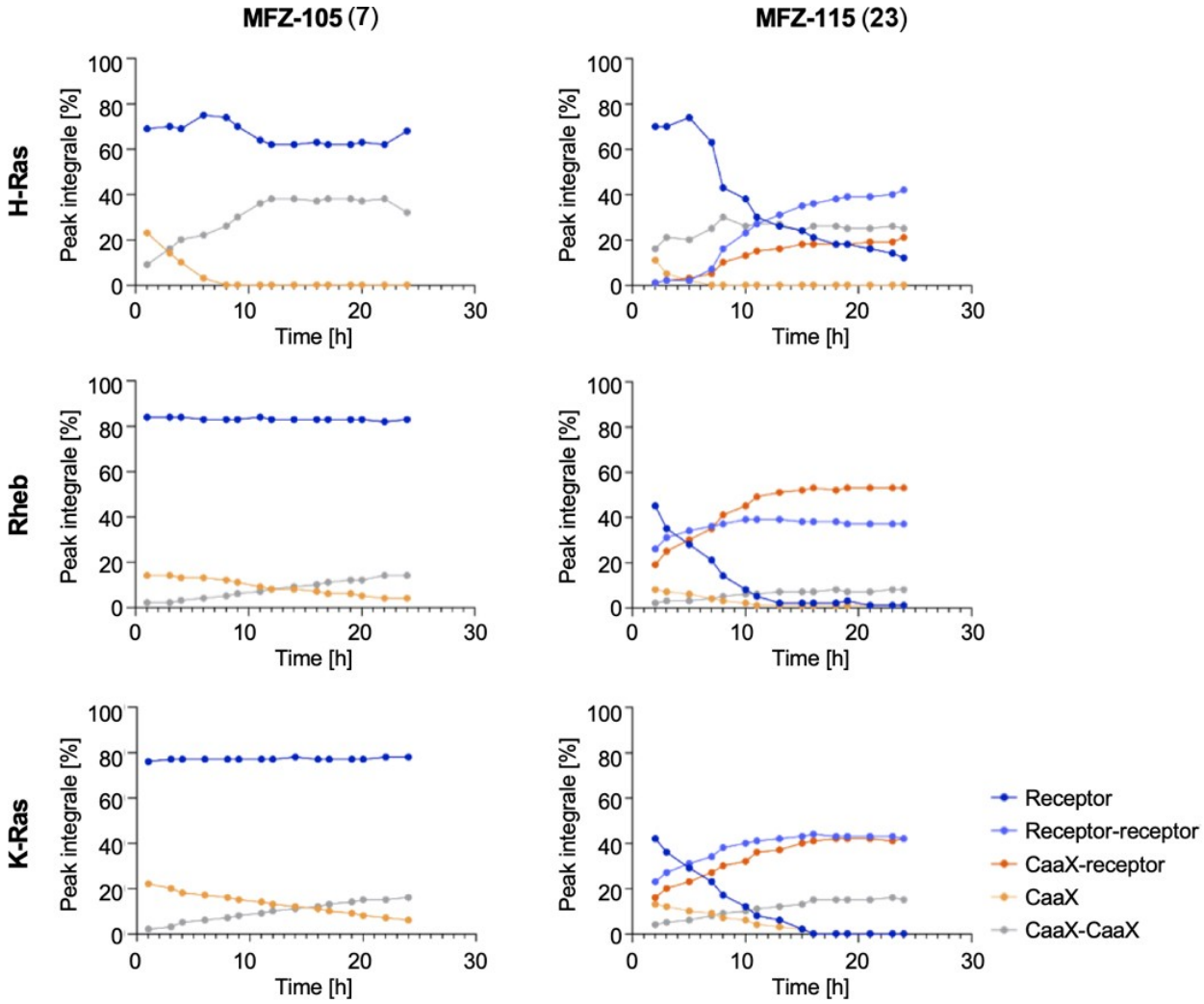

Figure 3. Incubation (LC–MS analysis) of C-terminal undecapeptides with acrylamide modified receptor MFZ-105 (**7**) and Thiol modified receptor MFZ-115 (**23**). C-terminal undecapeptides: Rheb, Ac-ASQGKSSCSVM-OH; H-Ras, Ac-PGCMSCKCVLS-OH; K-Ras, Ac-KKKSKTKCVIM-OH.

more remarkable that a LC–MS analysis of an incubation experiment with MFZ-115 (**23**) did not provide any hints on two- or threefold covalent modifications of the H-Ras 11mer. This underlines the suggested binding-mode (*vide infra*), which postulates the preformation of a strong ammonium salt-bridge with the C-terminal carboxylate of the Ras protein and the receptor guanidinopyrrole. Sequence and length of the molecular forceps then determine the selectivity for Cys residues in the neighborhood.

Mass spectrometric analysis of a K-Ras4B/MFZ-148 (27) conjugate

In order to show that the covalent modification is not limited to small C-terminal peptides, a conjugate consisting of K-Ras4B protein and molecular forceps MFZ-148 (**27**) was studied by electrospray ionization (ESI) mass spectrometry (MS). The results of the ESI MS experiments are illustrated in Figure 4. Due to the low signal to noise ratio, the charge cannot be derived from the isotopic pattern and needed to be calculated based on the average molecular weight of the protein. The charge state distribution of the MFZ-148 (**27**) modified K-Ras4B protein is shifted to higher masses in comparison to the unmodified K-Ras4B protein. The mass derived from the observed shift is 666.5 ± 50.6 Da, which is in good agreement with the molecular weight of receptor **27** (670 Da). These data demonstrate a covalent monofunctionalization of the K-Ras4B protein and thus confirm the results of the incubation experiments with the C-terminal 11mer peptides (Figure 3).

Molecular dynamics simulations of selected molecular receptors

In order to get more insight into the binding mode of our receptors, we first performed a MD simulation (500 ns simulation time, 0.15 M NaCl solution box) with full-length Rheb and

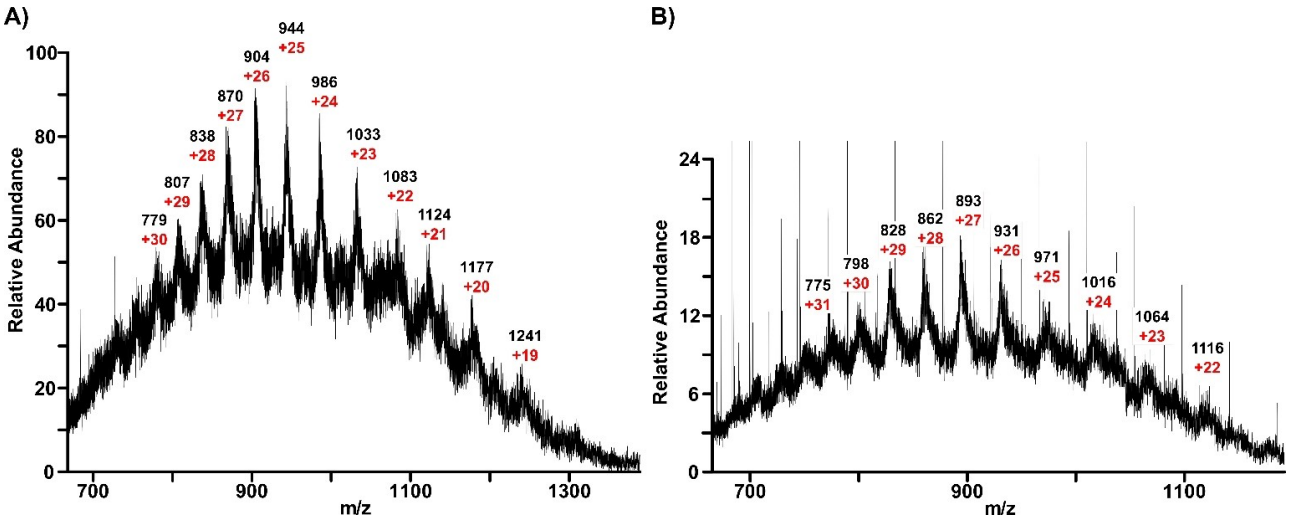

Figure 4. ESI-MS spectra of a K-Ras4B/MFZ-148 (**27**) conjugate. The mass of the charged entities are labelled in black and the respective charge in red. **A**) Spectrum of unmodified K-Ras4B protein. **B**) Spectrum of K-Ras4B modified with MFZ-148 (**27**).

the unmodified receptor MFZ-021 (**2**). It is well known, that the H-domains of Ras- and Rheb-proteins are flexible and solvent-exposed, an important prerequisite for molecular recognition by suitable receptor molecules.[36–38] In fact, protein-receptor interactions can be monitored for more than 90% of the simulation time. (Figure 5A). The dominant interaction is found between the C-terminal methionine and the guanidinio pyrrole head-group with minor contributions of the neighboring residues Val183, Ser182 und Cys181. The hypervariable region of Rheb remains highly flexible throughout the simulation. Remarkably, a small but significant cluster of structures shows tight interactions of the guanidiniopyrrole with both, the C-terminal Met184 and Asp171 (Figure 5B). This leads to a reorientation of the H-domain in such a way, that the C-terminus is placed in proximity to the switch 2 region (residues 60–76).[39] This particular arrangement of the G-domain and the hypervariable C-terminal region is additionally stabilized by hydrogen bridges to Val107 and water mediated to Arg7 and Ala173.

A 500 ns MD simulation (0.15 M NaCl solution) of MFZ-148 (**27**), the strongest thiol-based FTase inhibitor, and K-Ras4B (PDB: 4DSO, complemented with the C-terminal amino acids) revealed an analogous, dominant interaction with the C-terminal methionine (Figure 6A). However, the number of interactions between MFZ-148 (**27**) and Cys185, the target residue for sequence-selective covalent modification, is significantly higher compared to MFZ-021 (**2**, Figure 5A). This finding provides a plausible explanation for the good activity of MFZ-148 (**27**). The guanidinio moiety of receptor **27** also shows a significant interaction to Glu168, located in the transition from the α5-helix to the H-domain (Figure 6B). Altogether, the guanidiniopyrrole acts as a kind of molecular glue, which connects the hyperflexible C-terminus to the G-domain of K-Ras4B, alongside with a reduction of conformational freedom of the H-domain.

This special arrangement of the receptor-protein complex places the side-chain of one receptor lysine in close proximity to Glu49, which is reflected in the respective interaction

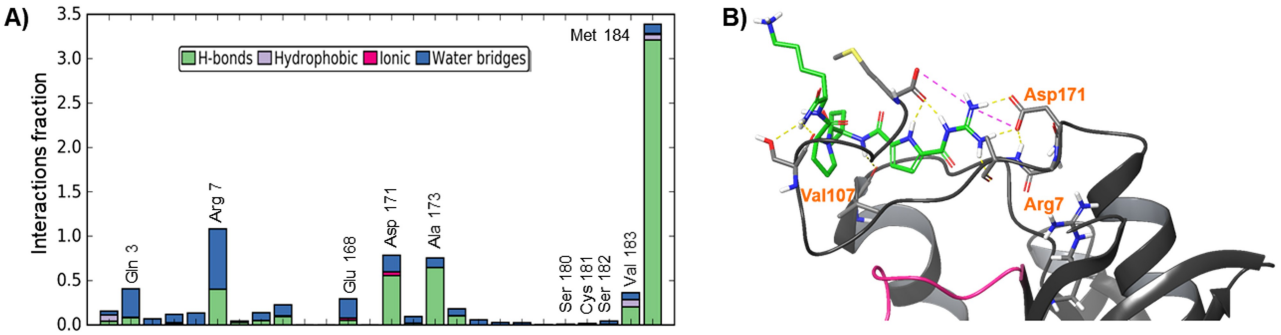

Figure 5. Molecular dynamics simulation of MFZ-021 (**2**) with full-length Rheb. **A)** Protein-ligand interaction diagram. **B**) Minor cluster with reorientation of the H-domain and interactions with G-domain residues. Magenta backbone: switch 2. The stacked bar charts are normalized over the course of the trajectory: for example, a value of 0.7 suggests that 70% of the simulation time, the specific interaction is maintained. Values over 1.0 are possible as some protein residues may make multiple contacts of same subtype with the ligand.

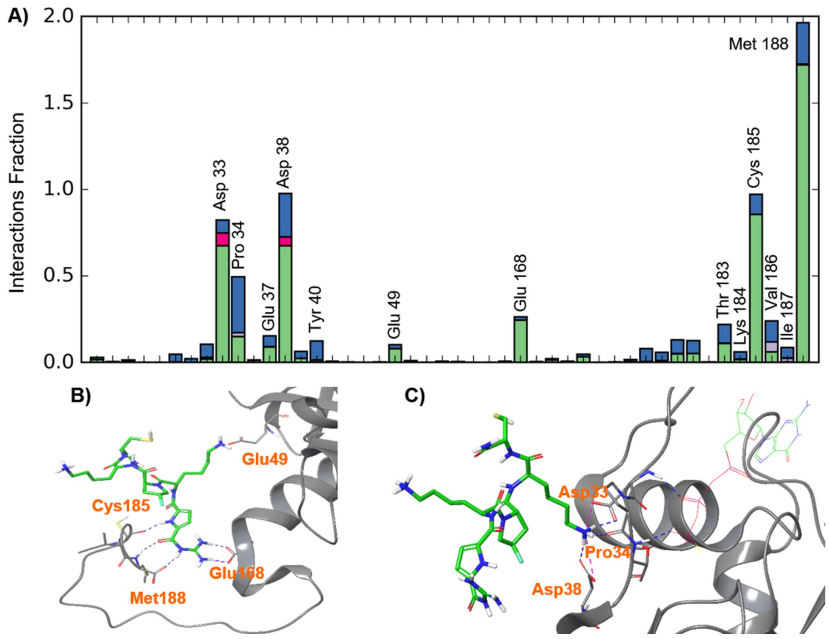

Figure 6. Dynamic simulation of K-Ras4B (PDB: 4DSO)/MFZ-148 (**27**) protein-ligand complex. **A**) Protein-ligand interaction diagram. **B**) Interactions of MFZ-148 (**27**) with K-Ras4B CaaX-box. **C**) Interactions of MFZ-148 (**27**) with switch 1 residues.

(Figure 6B). Noteworthy, after a simulation time of around 120 ns a second interaction cluster emerges, in which the switch 1 residues Asp33, Pro34 and Asp38 are involved (Figure. 6 C). These amino acids interact with the side-chain amino group of the second, more C-terminal receptor lysine. This cluster, however, is of no relevance since there are no cysteines for covalent modification in the reach of the molecular forceps.

Impact of CaaX-box receptors on cancer cell viability and RAS-dependent signaling

Biochemical FTase assays showed reduced FTase activity for several molecular forceps (Table 2). In a further step, we analyzed weather a reduction of Ras farnesylation results in suppression of cancer cell viability. Thus, K-Ras mutant $HCT116_{G13D}$ and $NCI–H358_{G12C}$ cancer cell lines were treated for 72 h with the covalent-modifying CaaX-box receptors under high serum conditions (Figure 7). Not really unexpected, the acrylamides were found inactive. Disappointingly, also the maleimides did not show any reduction in cell viability. We assume that the maleimides are either prematurely inactivated by glutathione or the labile thiosuccinimide linkage, which is known to be prone to hydrolysis, retro Michael addition and disulfide exchange reactions, is destroyed within the cell.[40] The two thiol-based compounds MFZ-115 (**23**) and MFZ-117 (**25**) showed a reduction of cell viability in the HCT116 cell line with IC_{50} concentrations varying between 445–538 μM and in the NCI–H358 cell line between 488–1741 μM. The strongest inhibition on cell viability was induced by the 4-fluoroproline derivative MFZ-148 (**27**) with IC_{50} of 312 μM (NCI-H358) and 413 μM (HCT116). The cellular IC_{50} values of CaaX-box receptors are up to 20-fold higher as required for suppression of Ras farnesylation in an aqueous setting. Obviously, our peptide-based molecular forceps have difficulties in penetrating the cellular plasma membrane due to their polarity.

The cellular uptake of peptides, is partially achieved by endocytic mechanisms. However, an endocytic uptake causes problems in the quantity of transported molecules and in the rate of their endosomal liberation, which makes it difficult to reach sufficient drug concentration at the target sites.[41,42]

Since the thiol-based CaaX-box receptors showed cellular killing, we addressed Ras-dependent downstream signaling on the MAPK and PI3 K/Akt kinase pathway. First, we analyzed the kinetics of Erk phosphorylation in human cancer cell lines. A short drug treatment of 2 h using MFZ-115 (**23**) did not influence the pErk status of HCT116 cells. In contrast, 20 h treatment reduced the Erk phosphorylation by 1.2-fold using 500 μM MFZ-115 (**23**, Figure 7). MFZ-117 (**25**) reduced Erk phosphorylation by 1.2-1.3 fold after 2 h treatment. A longer treatment of up to 20 h enhanced the downregulation of Erk phosphorylation of 1.4-fold (250 μM) to 1.6-fold using 500 μM MFZ-117 (**25**, Figure 7). A 20 h treatment with the covalent-binding CaaX-box receptors appeared to have the strongest effect on RAS downstream signaling. The exact half live of RAS proteins varies between tissues and cell types from 1-4 h in astrocytes, 9–20 h in pancreatic cancer cells.[43] Further, in pancreatic cancer cell lines, H-Ras shows a half live of 9–20 h, constitutive active forms of the protein even up to 42 h, while G12 V mutant K-Ras has a comparably short half live of 6–12 h.[44,45] Obviously, it takes time until embedded Ras is naturally degraded and the effect of reduced plasma membrane bound Ras kicks in. For further analyses 20 h drug incubation was applied.

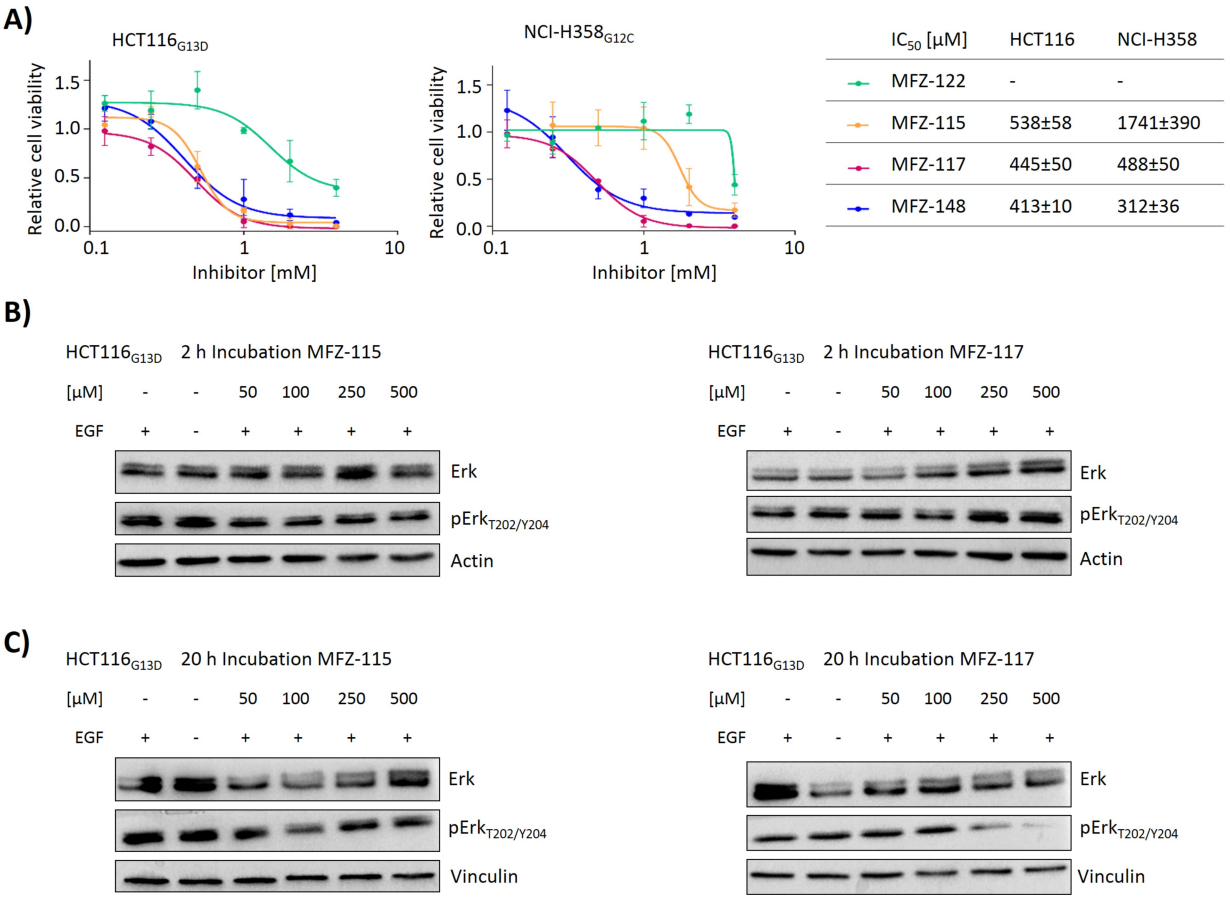

Figure 7. Thiol-based CaaX-box inhibitors reduce tumor cell viability. **A**) Dose response curves of HCT116 after 72 h incubation with MFZ-112 (**20**, no sigmoidal curve) MFZ-115 (**23**, $IC_{50} = 538 \pm 58$ µM), MFZ-117 (**25**, $IC_{50} = 445 \pm 50$ µM) and MFZ-148 (**27**, $IC_{50} = 413 \pm 10$ µM); Dose response curves of NCI–H358 after 72 h incubation with MFZ-112 (**20**, no sigmoidal curve fit), MFZ-115 (**23**, $IC_{50} = 1{,}741 \pm 0{,}39$ mM), MFZ-117 (**25**, $IC_{50} = 488 \pm 50$ µM) and MFZ-148 (**27**, $IC_{50} = 312 \pm 36$ µM). **B**, **C**) Western Blot analysis of RAS-dependent Erk phosphorylation of serum starved HCT116 cells after 2 h and 20 h incubation with potential CaaX-box inhibitors. Data is represented as mean ± SD, n = 3.

Thiol-based compounds were further tested on MAPK and PI3 K/Akt signaling in another human cancer cell model NCI-H358. After 20 h incubation with MFZ-115 (**23**) 50 µM induced 1.3-fold upregulation of pAkt, while 250 µM MFZ-115 (**23**) reduced the pAkt level by 1.12-fold. Erk phosphorylation is increased by 1.2-fold using 50 µM MFZ-115 (**23**). Higher concentrations reduce the pErk level by up to 1.6-fold. MFZ-117 (**25**) increases Akt phosphorylation using 50–100 µM 1.4-fold, 500 µM reduce Akt phosphorylation back to the baseline status of EGF stimulated cells. The pErk level does not increase by using low amounts of MFZ-115 (**23**), but decreased 1.3-fold applying 500 µM of the receptor (Figure 8A). Thiol-based CaaX-box receptors induced dose dependent decrease of Akt and Erk phosphorylation, implementing reduced RAS signaling. The 4-fluoroproline-derivate MFZ-148 (**27**) induced a slight upregulation of pAkt at 100–250 µM of 1.4-fold in NCI-H358 cells, higher doses of 500 µM MFZ-148 (**27**) reduced pErk level back to the baseline status. Erk phosphorylation decreased by up to 1.3-fold using 250–500 µM MFZ-148 (Figure 8B). HCT116 cells showed dose dependent decrease of Akt phosphorylation ranging from 1.1 (50 µM) to 1.4-fold (500 µM) reduction. The pErk level in HCT116 was also reduced by 1.2-fold by using 100–500 µM MFZ-148 (**27**).

As expected, molecular capsuling of the Ras C-terminus not only inhibits cancer cell viability but also modifies RAS-dependent cell signaling. Densiometric quantification of Western Blot results of the human cancer cell lines HCT116 and NCI-H358 showed increased Akt and Erk phosphorylation at lower receptor concentrations after 20 h treatment. Most likely, the cell is trying to regulate against this inhibition via upregulation of other RAS isoforms or associated proteins, leading to higher Akt/Erk phosphorylation at lower concentrations. With increasing receptor concentration within the cell, and the fact that the receptors could also bind to other Ras isoforms with lower affinity, cells fail to counter-regulate, which results in decreased activation of Ras-dependent downstream targets.

Conclusion

In this study we demonstrated that molecular forceps identified from combinatorial compound libraries can be significantly

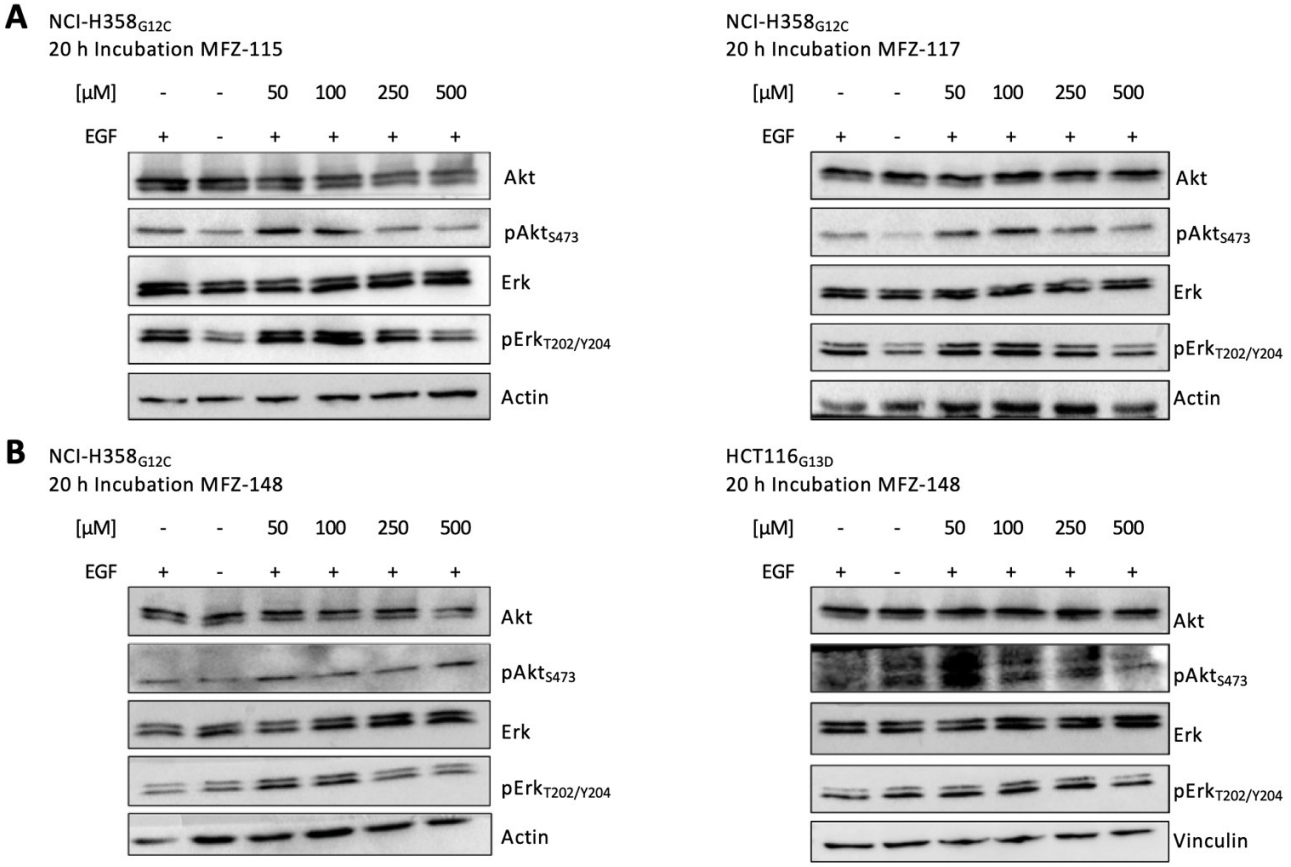

Figure 8. CaaX-box inhibitors modify RAS-dependent signaling cascades. **A**) Treatment of NCI–H358 cells with thiol-based inhibitors MFZ-115 (**23**) and MFZ-117 (**25**) for 20 h, followed by 10 min. stimulation von 100 ng/ml EGF under serum-free conditions. **B**) Western blot analysis of NCI–H358 and HCT116 cells after 20 h treatment with 4-fluoroproline derivate MFZ-148 (**27**). n = 3.

improved by adding covalent-modifying groups at appropriate positions. Those modified receptors alkylate or thiolate the CaaX-box cysteine and prevent subsequent farnesylation of Ras proteins with IC_{50} values in the low-micromolar range. This corresponds to an improvement by at least a factor of 10–20 compared to the original receptors. Remarkably, the molecular receptors MFZ-062 (**12**) and MFZ-066 (**16**) showed promising selectivities for the K-Ras4B CaaX-box while thiol MFZ-148 was found to be more selective for H-Ras by a factor of around two. Activity and selectivity strongly depend on the stereochemistry of the residue, carrying the covalent modifying group. This finding provides a promising basis for future molecular receptors with further improved activity and selectivity in favor of K-Ras4B. Molecular dynamics simulations postulate a formation of a strong salt-bridge between the guanidiniopyrrole of the molecular forceps and the C-terminal carboxylate prior to covalent modification of the Ras protein. For the first time, a significant effect of molecular encapsulation and covalent modification of Ras CaaX-boxes on cell viability and downstream-signaling could be demonstrated. However, cellular analyses of the peptidic CaaX-box receptors showed, that cell penetration is a limiting factor. Improved cellular uptake might be achieved via coupling of cell penetrating peptides (CPP), e.g. transactivating transcriptional activator (TAT) sequences from the immunodeficient virus 1 (HIV) sequences, to CaaX-box receptors. Several CPPs promote endocytosis for translocating molecules into a cell, while TAT is known to enhance a direct penetration of the plasma membrane, next to other proposed mechanisms, such as clathrin-dependent endocytosis.[46–48]

Experimental Section

Chemical syntheses

All derivatives of MFZ-021 (**2**), MFZ-022 (**3**) and MFZ-023 (**5**) were prepared by standard solid-phase chemistry with Rink-amide as solid support, following standard solid phase synthesis protocols. Coupling of amino acids was carried out twice with either PyBOP, HBTU or TBTU in similar yields. The solid-phase acylation with acryloyl chloride turned out to be more critical due to low reaction rates and concomitant formation of by-products. Best results were obtained by a single coupling of 2.5 eq acryloyl chloride and 5.0 eq NEt_3 in DMF for 5 h at room temperature. Coupling of dioxopyrrolo acetic acid (2.5 eq) was accomplished by preincubation with PyBOP (2.5 eq)/DIPEA (5.0 eq) for 15 min in DMF and subsequent addition to the resin. Overall, five series of compounds were prepared, differing by the number and stereochemistry of residues and by the type of covalent-modifying group.

H_2NCO-*D*-Lys(Acr)-*L*-Pro-*L*–Lys-hg, MFZ-102 (**6**): HPLC purity: 100%. HRMS (ESI): calcd. for $C_{27}H_{43}N_{10}O_6$ $[M+H]^+$ 603.3362; found: 603.3355. H_2NCO-*D*-Lys(Acr)-GABA-*L*–Lys-hg, MFZ-105 (**7**): HPLC purity: 100%. HRMS (ESI): calcd. for $C_{26}H_{43}N_{10}O_6$ $[M+H]^+$ 591.3362; found: 591.3371. H_2NCO-*L*-Lys(Acr)-*D*-Lys-*L*-Pro-AC5 C-hg, MFZ-039 (**8**): HPLC purity: 95%. HRMS (ESI): calcd. for $C_{33}H_{52}N_{11}O_7$ $[M+H]^+$ 714.4046; found: 714.4045. H_2NCO-*D*-Lys(Acr)-*D*-Lys-*L*-Pro-AC5 C-hg, MFZ-040 (**9**): HPLC purity: 88%. HRMS (ESI): calcd. for $C_{33}H_{52}N_{11}O_7$ $[M+H]^+$ 714.4046; found: 714.4033. H_2NCO-*L*–Lys(Acr)-*D*-Lys-*L*-Pro-*L*–Lys-hg, MFZ-041 (**10**): HPLC purity: 100%. HRMS (ESI): calcd. for $C_{33}H_{55}N_{12}O_7$ $[M+H]^+$ 731.4311; found: 731.4312. H_2NCO-*D*-Lys(Acr)-*D*-Lys-*L*-Pro-*L*–Lys-hg, MFZ-042 (**11**): HPLC purity: 93%. HRMS (ESI): calcd. for $C_{33}H_{55}N_{12}O_7$ $[M+H]^+$ 731.4311; found: 731.4316. H_2NCO-*L*–Lys(Gly-Mi)-*D*-Lys-*L*-Pro-AC5 C-hg, MFZ-062 (**12**): HPLC purity: 95%. HRMS (ESI): calcd. for $C_{36}H_{53}N_{12}O_9$ $[M+H]^+$ 797.4053; found: 797.4051. H_2NCO-*D*-Lys(Gly-Mi)-*D*-Lys-*L*-Pro-AC5 C-hg, MFZ-063 (**13**): HPLC purity: 100%. HRMS (ESI): calcd. for $C_{36}H_{53}N_{12}O_9$ $[M+H]^+$ 797.4053; found: 797.4057. H_2NCO-*L*–Lys(Gly-Mi)-*D*-Lys-*L*-Pro-*L*–Lys-hg, MFZ-064 (**14**): HPLC purity: 98%. HRMS (ESI): calcd. for $C_{36}H_{56}N_{13}O_9$ $[M+H]^+$ 814.4318; found: 814.4317. H_2NCO-*D*-Lys(Gly-Mi)-*D*-Lys-*L*-Pro-*L*–Lys-hg, MFZ-065 (**15**): HPLC purity: 98%. HRMS (ESI): calcd. for $C_{36}H_{56}N_{13}O_9$ $[M+H]^+$ 814.4318; found: 814.4319. H_2NCO-*L*–Lys(Gly-Mi)-*D*-Lys-GABA-*L*–Lys-hg, MFZ-066 (**16**): HPLC purity: 92%. HRMS (ESI): calcd. for $C_{35}H_{56}N_{13}O_9$ $[M+H]^+$ 802.4318; found: 802.4315. H_2NCO-*D*-Lys(Gly-Mi)-*D*-Lys-GABA-*L*–Lys-hg, MFZ-067 (**17**): HPLC purity: 93%. HRMS (ESI): calcd. for $C_{35}H_{56}N_{13}O_9$ $[M+H]^+$ 802.4318; found: 802.4319. H_2NCO-*D*-Cys-*L*-Pro-AC5 C-hg, MFZ-110 (**18**): HPLC purity: 91%. HRMS (ESI): calcd. for $C_{21}H_{30}N_8NaO_5S$ $[M+Na]^+$ 529.1952; found: 529.1965. H_2NCO-*D*-Cys -*L*-Pro-*L*–Lys-hg, MFZ-111 (**19**): HPLC purity: >99%. HRMS (ESI): calcd. for $C_{21}H_{34}N_9O_5S$ $[M+H]^+$ 524.2398; found: 524.2399. H_2NCO-*D*-Cys-GABA-*L*–Lys-hg, MFZ-112 (**20**): HPLC purity: 98%. HRMS (ESI): calcd. for $C_{20}H_{34}N_9O_5S$ $[M+H]^+$ 512.2398; found: 512.2396. H_2NCO-*L*–Cys-*D*-Lys-*L*-Pro-AC5 C-hg, MFZ-113 (**21**): HPLC purity: 98%. HRMS (ESI): calcd. for $C_{27}H_{42}N_{10}NaO_6S$ $[M+Na]^+$ 657.2902; found: 657.2895. H_2NCO-*D*-Cys-*D*-Lys-*L*-Pro-AC5 C-hg, MFZ-114 (**22**): HPLC purity: 99%. HRMS (ESI): calcd. for $C_{27}H_{42}N_{10}NaO_6S$ $[M+Na]^+$ 657.2902; found: 657.2903. H_2NCO-*L*–Cys-*D*-Lys-*L*-Pro-*L*–Lys-hg, MFZ-115 (**23**): HPLC purity: 95%. HRMS (ESI): calcd. for $C_{27}H_{46}N_{11}O_6S$ $[M+H]^+$ 652.3348; found: 652.3367. H_2NCO-*D*-Cys-*D*-Lys-*L*-Pro-*L*–Lys-hg, MFZ-116 (**24**): HPLC purity: >99%. HRMS (ESI): calcd. for $C_{27}H_{46}N_{11}O_6S$ $[M+H]^+$ 652.3348; found: 652.3361. H_2NCO-*L*–Cys-*D*-Lys-GABA-*L*–Lys-hg, MFZ-117 (**25**): HPLC purity: 96%. HRMS (ESI): calcd. for $C_{26}H_{46}N_{11}O_6S$ $[M+H]^+$ 640.3348; found: 640.3349. H_2NCO-*D*-Cys-*D*-Lys-GABA-*L*–Lys-hg, MFZ-118 (**26**): HPLC purity: 95%. HRMS (ESI): calcd. for $C_{26}H_{46}N_{11}O_6S$ $[M+H]^+$ 640.3348; found: 640.3349. H_2NCO-*L*–Cys-*D*-Lys-L-Pro(4-F)-*L*–Lys-hg, MFZ-148 (**27**): HPLC purity: >99%. HRMS (ESI): calcd. for $C_{27}H_{45}FN_{11}O_6S$ $[M+H]^+$ 670.3254; found: 670.3255.

HPLC and HPLC-MS analyses of 11-mer C-termini and molecular receptors

A stock solution of the receptor in DMSO (1.0 μmol, 10 μL, 0.1 M) and a stock solution of the K-Ras4B CaaX Peptide in DMSO (1.0 μmol, 10 μL, 0.1 M) were added to PBS (980 μL) buffer and mixed by careful pipetting. The reactions were shaken at rt and samples were taken and lyophilized after 30 min, 1 h, 2 h, 4 h, 8 h and 24 h. The analyses were performed on an Agilent 1220 Infinity system and a Shimadzu LC-2030 C HPLC-MS(ESI) system, using an acetonitrile/water (0.1% TFA) gradient.

Protein mass spectrometry

10 mg of K-Ras4B protein in 1 ml PBS buffer (pH 7.4, 1 mM DTT) were exchanged via Zeba™ Spin Desalting columns (Thermo Fisher™) into PBS buffer without reducing agent DTT. The covalent binding was performed by incubating 10 mg of K-Ras4B in 1 ml PBS buffer pH 7.4 with a 20-fold excess of MFZ-148 (**27**) for 16 h at 4 °C. After the incubation, the protein was purified by gel filtration with a Superdex® 75 10/300 GL (GE Healthcare). Prior to lyophilization, the buffer was exchanged into ddH2O via Zeba™ Spin Desalting columns. The lyophilization was performed in a VaCo 5 laboratory freeze dryer (ZiRBUS Technology) for 20 h. The samples were resuspended in 0.1% formic acid for a final concentration of 0.1 mM. A Thermo LTQ XL Orbitrap (Thermo Fisher™) was used for direct infusion of the proteins. The heated desolvation capillary was set to 200 °C and a spray voltage of 1.8 kV was supplied. In the tune file the LTQ Orbitrap was set to the following parameters (R 60,000; IT = 500 ms; AGC Target = 1,000,000).

Farnesyltransferase assay

A fluorescence based farnesyltransferase assay, described by Pompliano,[49] was applied to test the compounds for an inhibitory effect on farnesylation. Specificity for K-Ras, H-Ras or Rheb was checked by using different dansylated substrate peptides (Dans-GCVLS for H-Ras, dans-GCVIM for K-Ras and dans-TKCSVM for RheB). The assay was miniaturized to 384 well format (10 μl final volume). Final assay concentrations were as follows: 5 nM FTase for H-Ras and RheB, 20 nM for K-Ras. Concentration of all substrates was 5 μM. Enzyme reactions were performed in 50 mM Tris buffer pH 7,5 containing 10 μM $ZnCl_2$, 5 mM $MgCl_2$ and 0,2% Octyl-β-(*D*)-Glucopyranoside. The assay buffer did not contain any reducing agents such as DTT, to avoid reduction of the disulfide bond, which covalently links the molecular receptor to the CaaX-box cysteine. Compound transfer to the assay plate was done by using an acoustic dispenser (Echo, Labcyte). For the generation of dose response curves a concentration range from 30 to 0,05 μM was used. Compounds were transferred to the plate already containing the substrate and farnesylpyrophosphate. After pre-incubation for 15 minutes the enzymatic reaction was started through addition of farnesyltransferase followed by an incubation at 30 °C for 3 h. After that the plate was measured with a suitable plate reader (Victor, PerkinElmer); exc. wavelength: 355 nm, em. wavelength: 535 nm. All 3 assays fulfill standard assay QC criteria like z'-factor >0,5 and signal to noise ratio >12. Before actual compound testing an additional validation step was done. For that the IC_{50} values of known FTase inhibitors like Tiparfinib were determined (8-point dose response curves, lowest compound concentration up to 2,5 nM). For further routine check of the assay performance the IC_{50} value of the Tipifarnib stereoisomer was determined (Supporting Information).

Cells and cell culture

KRAS mutant human HCT116 colon cancer cells and NCI–H358 NSCLC cells were maintained from the American Type Culture Collection (ATCC). HCT116 was cultured in Mc Coy's 5 A Medium (Sigma-Aldrich) supplemented with 10% FCS, 1% L-Glutamine (Gibco, Fisher Scientific) and 1% Penicillin/Streptomycin (Gibco, Fisher Scientific). NCI–H358 cells were cultured in RPMI Medium 1640 (Gibco, Fisher Scientific) supplemented with 10% FCS and 1% Penicillin/Streptomycin. The cells incubated at 37 °C, 5% CO_2 condition.

XTT cytotoxicity assay

HCT116 and NCI-H358 were seeded at defined cell numbers in 96 well plates. 24 h after seeding, cells were treated with CaaX-box receptors dissolved in H_2O at maximal concentrations of 4 mM. After 72 h incubation at 37 °C, 5% CO_2 condition XTT assay was performed according to manufactures protocol (Invitrogen, Fisher Scientific). Cell viability was measured in a Multimode Plate Reader at 450 nm, and 630 nm reference wavelength. Sigmoidal dose response curves were fitted using Prism8 Software (GraphPad) and half-maximal inhibiting concentrations (IC_{50}) were determined.

Western blot

Cells were seeded in defined cell numbers 24 h prior to the treatment with potential CaaX-box inhibitors. Cells were washed twice with PBS and incubated under serum-free conditions 2–20 h with potential CaaX-box receptors. Before lysis, cells were stimulated with 100 ng/ml EGF for 10 min. Proteins were extracted, separated by SDS-PAGE and transferred on 0.45 μM nitrocellulose membranes. The membranes were probed over night at 4 °C with primary antibody. Following primary antibodies were used: Erk (cat. 4695), pErk (cat. 4377), Akt (cat. 4691), pAkt (cat. 4058) all Cell Signaling. Actin (cat. 691001, MP Biomedicals, Fisher Scientific) and vinculin (cat. sc-25336, Santa Cruz) served as loading controls. Membranes were incubated with appropriate horseradish peroxidase conjugated secondary antibodies, allowing signal visualization via enhanced chemiluminescence with Pierce ECL Western Blotting Substrate (Fisher Scientific). Densiometric quantification of protein signals were quantified using ImageJ Software.[50] All protein signals were normalized to actin or vinculin, then phosphoprotein signals were normalized to total protein expression, foldchanges were calculated.

Molecular modeling

Molecular dynamics simulations were performed with Desmond as a component of the Schrödinger molecular modeling package 2018-1. Conditions for all MD simulations were: box shape, orthorhombic; solvent model, SPC, solvent, 0.15 M NaCl; recording interval, 5.0 ps; energy, 1.2; Temp, 300 K; pressure, 1.01325 bar.

Funding sources

This work was supported by the European Regional Development Fund (EFRE-0800945, LS-1-2-001a, RIST).

Acknowledgements

The authors thank I. Polanz, S. Bettinger, and A. Siebert for measuring HRMS and NMR spectra. Open access funding enabled and organized by Projekt DEAL.

Conflict of Interest

The authors declare no conflict of interest.

Keywords: Ras protein · K-Ras4B · molecular recognition · CaaX-box · covalent inhibitor

[1] J. Rudolph, D. Stokoe, *Angew. Chem. Int. Ed.* **2014**, *53*, 3777–3779; *Angew. Chem.* **2014**, *126*, 3851–3853.
[2] L. M. Jarvis, *C&EN* **2016**, *94*, 28–33.
[3] B. Papke, C. J. Der, *Science (80-.).* **2017**, *355*, 1158–1163.
[4] P. Liu, Y. Wang, X. Li, *Acta Pharm. Sin. B* **2019**, *9*, 871–879.
[5] P.-J. Aspuria, F. Tamanoi, *Cell. Signalling* **2004**, *16*, 1105–1112.
[6] K. J. Mavrakis, H. Zhu, R. L. A. Silva, J. R. Mills, J. Teruya-Feldstein, S. W. Lowe, W. Tam, J. Pelletier, H.-G. Wendel, *Genes Dev.* **2008**, *22*, 2178–2188.
[7] Z. H. Lu, M. B. Shvartsman, A. Y. Lee, J. M. Shao, M. M. Murray, R. D. Kladney, D. Fan, S. Krajewski, G. G. Chiang, G. B. Mills, et al., *Cancer Res.* **2010**, *70*, 3287–3298.
[8] A. D. Cox, S. W. Fesik, A. C. Kimmelman, J. Luo, C. J. Der, *Nat. Rev. Drug Discovery* **2014**, *13*, 828–851.
[9] C. V. Dang, E. P. Reddy, K. M. Shokat, L. Soucek, *Nat. Rev. Cancer* **2017**, *17*, 502–508.
[10] H. Ledford, *Nature* **2015**, *520*, 278–280.
[11] J. L. Gray, F. Delft, P. E. Brennan, *Angew. Chem. Int. Ed.* **2020**, *59*, 6342–6366; *Angew. Chem.* **2020**, *132*, 6402–6428.
[12] D. Kessler, M. Gmachl, A. Mantoulidis, L. J. Martin, A. Zoephel, M. Mayer, A. Gollner, D. Covini, S. Fischer, T. Gerstberger, et al., *Proc. Nat. Acad. Sci.* **2019**, *116*, 15823–15829.
[13] S. Lu, H. Jang, S. Gu, J. Zhang, R. Nussinov, *Chem. Soc. Rev.* **2016**, *45*, 4929–4952.
[14] A. R. Moore, S. C. Rosenberg, F. McCormick, S. Malek, *Nat. Rev. Drug Discovery* **2020**, *19*, 533–552.
[15] A. Mullard, *Nat. Rev. Drug Discovery* **2019**, *18*, 887–891.
[16] A. Cruz-Migoni, P. Canning, C. E. Quevedo, C. J. R. Bataille, N. Bery, A. Miller, A. J. Russell, S. E. V. Phillips, S. B. Carr, T. H. Rabbitts, *Proc. Nat. Acad. Sci.* **2019**, *116*, 2545–2550.
[17] S. J. Lynch, H. Snitkin, I. Gumper, M. R. Philips, D. Sabatini, A. Pellicer, *J. Cell. Physiol.* **2015**, *230*, 610–619.
[18] I. Ahearn, M. Zhou, M. R. Philips, *Cold Spring Harbor Perspect. Med.* **2018**, *8*, a031484.
[19] S. Dharmaiah, L. Bindu, T. H. Tran, W. K. Gillette, P. H. Frank, R. Ghirlando, D. V. Nissley, D. Esposito, F. McCormick, A. G. Stephen, et al., *Proc. Nat. Acad. Sci.* **2016**, *113*, E6766–E6775.
[20] N. Ye, Q. Xu, W. Li, P. Wang, J. Zhou, *Curr. Top. Med. Chem.* **2019**, *19*, 2114–2127.
[21] E. K. Rowinsky, J. J. Windle, D. D. Von Hoff, *J. Clin. Oncol.* **1999**, *17*, 3631–3652.
[22] D. L. Dong, R. Liu, R. Sherlock, M. H. Wigler, H. P. Nestler, *Chem. Biol.* **1999**, *6*, 133–141.
[23] C. Schmuck, D. Rupprecht, M. Junkers, T. Schrader, *Chem. Eur. J.* **2007**, *13*, 6864–6873.
[24] C. Schmuck, L. Geiger, *J. Am. Chem. Soc.* **2004**, *126*, 8898–8899.
[25] C. Schmuck, *Chem. Eur. J.* **2000**, *6*, 709–718.
[26] P. M. Düppe, T. Tran Thi Phuong, J. Autzen, M. Schöpel, K. T. Yip, R. Stoll, J. Scherkenbeck, *ACS Chem. Biol.* **2014**, *9*, 1755–1763.
[27] M. Schöpel, K. F. G. Jockers, P. M. Düppe, J. Autzen, V. N. Potheraveedu, S. Ince, K. T. Yip, R. Heumann, C. Herrmann, J. Scherkenbeck, et al., *J. Med. Chem.* **2013**, *56*, 9664–72.
[28] K. E. Hightower, C. Huang, P. J. Casey, C. A. Fierke, *Biochemistry* **1998**, *37*, 15555–15562.
[29] F. Sutanto, M. Konstantinidou, A. Dömling, *RSC Med. Chem.* **2020**, *11*, 876–884.
[30] A. K. Ghosh, I. Samanta, A. Mondal, W. R. Liu, *ChemMedChem* **2019**, *14*, 889–906.
[31] M. Gehringer, S. A. Laufer, *J. Med. Chem.* **2019**, *62*, 5673–5724.
[32] R. A. Bauer, *Drug Discovery Today* **2015**, *20*, 1061–1073.
[33] O. Koniev, A. Wagner, *Chem. Soc. Rev.* **2015**, *44*, 5495–5551.
[34] S. B. Gunnoo, A. Madder, *ChemBioChem* **2016**, *17*, 529–553.
[35] P. A. Jackson, J. C. Widen, D. A. Harki, K. M. Brummond, *J. Med. Chem.* **2017**, *60*, 839–885.
[36] Y. Yu, S. Li, X. Xu, Y. Li, K. Guan, E. Arnold, J. Ding, *J. Biol. Chem.* **2005**, *280*, 17093–17100.
[37] A. A. Gorfe, M. Hanzal-Bayer, D. Abankwa, J. F. Hancock, J. A. McCammon, *J. Med. Chem.* **2007**, *50*, 674–684.
[38] R. Thapar, J. G. Williams, S. L. Campbell, *J. Mol. Biol.* **2004**, *343*, 1391–1408.

[39] T. S. Chavan, H. Jang, L. Khavrutskii, S. J. Abraham, A. Banerjee, B. C. Freed, L. Johannessen, S. G. Tarasov, V. Gaponenko, R. Nussinov, et al., *Biophys. J.* **2015**, *109*, 2602–2613.
[40] K. Renault, J. W. Fredy, P.-Y. Renard, C. Sabot, *Bioconjugate Chem.* **2018**, *29*, 2497–2513.
[41] V. V. Vlassov, L. A. Blakireva, L. A. Yakubov, *Biochim. Biophys. Acta Rev. Biomembr.* **1994**, *1197*, 95–108.
[42] J. Oehlke, A. Scheller, B. Wiesner, E. Krause, M. Beyermann, E. Klauschenz, M. Melzig, M. Bienert, *Biochim. Biophys. Acta Biomembr.* **1998**, *1414*, 127–139.
[43] S. Messina, E. Di Zazzo, B. Moncharmont, *Antioxidants* **2017**, *6*, 48.
[44] C. A. Ellis, G. Clark, *Cell. Signalling* **2000**, *12*, 425–434.
[45] L. S. Ulsh, T. Y. Shih, *Mol. Cell. Biol.* **1984**, *4*, 1647–1652.
[46] E. Vivès, P. Brodin, B. Lebleu, *J. Biol. Chem.* **1997**, *272*, 16010–16017.
[47] O. Zelphati, F. C. Szoka, *Pharm. Res.* **1996**, *13*, 1367–72.
[48] K. Wagstaff, D. Jans, *Curr. Med. Chem.* **2006**, *13*, 1371–1387.
[49] D. L. Pompliano, R. P. Gomez, N. J. Anthony, *J. Am. Chem. Soc.* **1992**, *114*, 7945–7946.
[50] J. Schindelin, I. Arganda-Carreras, E. Frise, V. Kaynig, M. Longair, T. Pietzsch, S. Preibisch, C. Rueden, S. Saalfeld, B. Schmid, et al., *Nat. Methods* **2012**, *9*, 676–682.

Manuscript received: March 8, 2021
Accepted manuscript online: April 26, 2021
Version of record online: May 19, 2021